Vol 459|28 May 2009|doi:10.1038/nature08005

LETTERS

Synthesizing arbitrary quantum states in a superconducting resonator

Max Hofheinz[1], H. Wang[1], M. Ansmann[1], Radoslaw C. Bialczak[1], Erik Lucero[1], M. Neeley[1], A. D. O'Connell[1], D. Sank[1], J. Wenner[1], John M. Martinis[1] & A. N. Cleland[1]

The superposition principle is a fundamental tenet of quantum mechanics. It allows a quantum system to be 'in two places at the same time', because the quantum state of a physical system can simultaneously include measurably different physical states. The preparation and use of such superposed states forms the basis of quantum computation and simulation[1]. The creation of complex superpositions in harmonic systems (such as the motional state of trapped ions[2], microwave resonators[3–5] or optical cavities[6]) has presented a significant challenge because it cannot be achieved with classical control signals. Here we demonstrate the preparation and measurement of arbitrary quantum states in an electromagnetic resonator, superposing states with different numbers of photons in a completely controlled and deterministic manner. We synthesize the states using a superconducting phase qubit to phase-coherently pump photons into the resonator, making use of an algorithm[7] that generalizes a previously demonstrated method of generating photon number (Fock) states in a resonator[8]. We completely characterize the resonator quantum state using Wigner tomography, which is equivalent to measuring the resonator's full density matrix.

The quantum state of a resonator is extraordinarily rich, with infinitely many energy levels, of which each can have a non-zero amplitude. However, this richness is difficult to access when driving a resonator with a classical signal, as the two adjustable parameters of an on-resonant drive, the amplitude and the phase, give very limited control. Creating an arbitrary quantum state instead requires a nonlinear element and a control scheme with many parameters. Here we demonstrate quantum state generation in a resonator by interposing a highly nonlinear Josephson phase qubit[9] between a superconducting resonator and a classical signal. A qubit[4,5,10–14] has two quantum degrees of freedom, the relative amplitude and phase of its ground $|g\rangle$ and excited $|e\rangle$ energy eigenstates. This simplicity allows full quantum control of a qubit with a classical signal[15]. By following a sequence of steps developed for trapped ions[2,7] (and later adapted to charge qubits[16]), where each step involves creating a particular qubit state and then having the qubit interact with the resonator for a controlled time, we synthesize arbitrary states in the resonator. The preparation is deterministic, unlike methods involving probabilistic projective measurements[17]. After the preparation, we analyse the resonator state using Wigner tomography[18–22], mapping out the Wigner quasi-probability distribution[23,24], from which we extract the resonator's full density matrix.

The quantum circuit we used is shown in Fig. 1a. The phase qubit is capacitively coupled to a superconducting coplanar waveguide resonator, and the circuit includes control lines for the qubit and resonator, and a qubit measurement circuit described elsewhere[25]. This circuit is similar to that used previously to generate Fock states in a resonator[8]; here, however, most of the superconducting wiring is made of rhenium in place of aluminium, and we removed unnecessary dielectric, reducing dissipative elements in the circuit.

The qubit frequency $\omega_q/2\pi$ can be externally adjusted, whereas the resonator frequency $\omega_r/2\pi = 6.570$ GHz is fixed. This allows us to

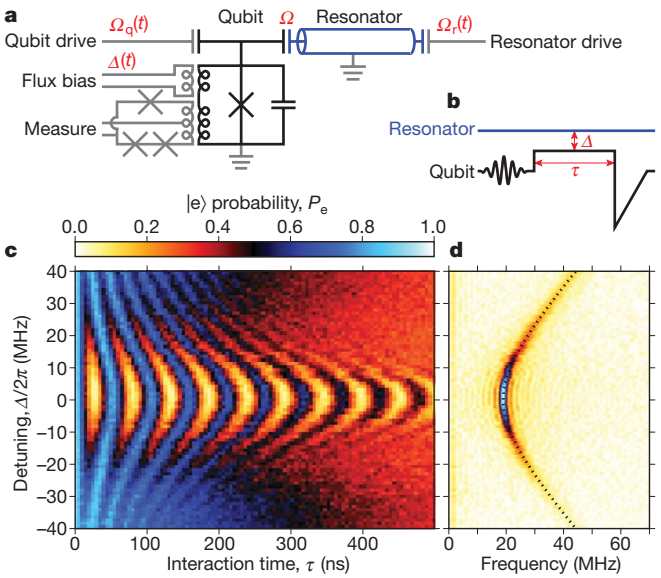

Figure 1 | Circuit diagram and one photon Rabi-swap oscillations between qubit and resonator. a, The qubit (black) is made from a Josephson junction (cross) and a capacitor, biased through a shunting inductor. The qubit detuning Δ is adjusted through a flux bias coil, and the qubit state is read out by a three-Josephson-junction superconducting quantum interference device (SQUID). The coplanar waveguide resonator (blue) has fixed capacitive coupling Ω to the qubit, and small capacitors couple external microwave signals Ω_q and Ω_r to the qubit and resonator. The device was measured in a dilution refrigerator at 25 mK. The qubit relaxation and dephasing times were respectively $T_{1,q} \approx 650$ ns and $T_{2,q} \approx 150$ ns, and the resonator relaxation time was $T_{1,r} \approx 3.5$ μs with no measurable dephasing. **b**, Schematic of Rabi-swap pulse sequence. The qubit starts in its ground state, detuned at its typical off-resonance point by $\Delta_{off}/2\pi = -463\,\text{MHz} \approx -25\Omega/2\pi$ from the resonator. A resonant qubit microwave π-pulse brings the qubit to its excited state $|e\rangle$, injecting one quantum of energy into the system. A flux bias pulse reduces the qubit detuning Δ from the resonator for a controlled time τ, and the qubit state is then measured with a current pulse. **c**, Excited state probability P_e versus detuning Δ and interaction time τ. P_e is obtained by averaging 600 repetitions. **d**, Fourier transform of data in **c**, showing the expected hyperbolic relation between detuning Δ and swap frequency $\sqrt{\Omega^2+\Delta^2}/2\pi$ (dotted line), and the expected fall-off in probability (colour scale). Resonance $\Delta = 0$ corresponds to lowest swap frequency and maximum probability amplitude.

[1]Department of Physics, University of California, Santa Barbara, California 93106, USA.

Table 1 | Sequence to generate the resonator state $|\psi\rangle = |1\rangle + i|3\rangle$

Sequence of states, operations	Operational parameter	System state, parameter value
$\|\psi\rangle$		$\|g\rangle(0.707\|1\rangle+0.707i\|3\rangle)$
S_3	$\tau_3\Omega$	1.81
Q_3	q_3	3.14
$\|\psi_2\rangle$		$\|g\rangle(-0.557i\|0\rangle+0.707\|2\rangle)+0.436\|e\rangle\|1\rangle$
Z_2	$t_2\Delta$	4.71
S_2	$\tau_2\Omega$	1.44
Q_2	q_2	$-2.09-2.34i$
$\|\psi_1\rangle$		$(0.553-0.62i)\|g\rangle\|1\rangle-(0.371+0.416i)\|e\rangle\|0\rangle$
Z_1	$t_1\Delta$	3.26
S_1	$\tau_1\Omega$	1.96
Q_1	q_1	$-2.71-1.59i$
$\|\psi_0\rangle$		$(0.197-0.98i)\|g\rangle\|0\rangle$

This resonator state is used for the measurements described in Fig. 2. The sequence is computed top to bottom, but applied bottom to top. The area and phase for the nth qubit drive Q_n is $q_n = \int \Omega_q(t)e^{i\Delta_{off}t}dt$ ($t = 0$ being the time when the qubit is tuned into resonance directly after the swap Q_n), the time on-resonance for the qubit–resonator swap operation S_n is τ_n, and the time off-resonance (mod $2\pi/\Delta$) for the phase rotation Z_n is t_n. We note that the initial state $|\psi_0\rangle$ differs by an overall phase factor from the ground state $|g\rangle|0\rangle$, but this is not detectable. State descriptions are shown bold; operations are not in bold.

describe the system with a Hamiltonian in the resonator rotating frame, so that the resonator states have zero frequency:

$$\frac{H}{\hbar} = \Delta(t)\sigma_+\sigma_- + \left(\frac{\Omega}{2}\sigma_+ a + \frac{\Omega_q(t)}{2}\sigma_+ + \frac{\Omega_r(t)}{2}a^\dagger\right) + \text{h.c.} \quad (1)$$

Here σ_+ and σ_- ($a^\dagger$ and a) are the qubit (resonator) raising and lowering operators, and h.c. is the Hermitian conjugate of the terms in parentheses. The first term is the qubit energy, which appears as the qubit–resonator detuning $\Delta(t) = \omega_q(t) - \omega_r$. The first term in the parentheses gives the qubit–resonator interaction, proportional to the fixed interaction strength $\Omega/2\pi = 19$ MHz, while the second and third terms give the effect of the external microwave drive signals applied to the qubit and resonator; these parameters $\Omega_q(t)$ and $\Omega_r(t)$ are complex to account for amplitude and phase. All control signals in equation (1) vary on a ~2 ns timescale, long compared to $2\pi/\omega_r$, so counter-rotating terms in equation (1) are neglected.

Although the coupling Ω is fixed, we control the qubit–resonator interaction by adjusting the qubit frequency between two operating points, one with qubit and resonator exactly on resonance ($\Delta_{on} = 0$), the other with the qubit well off-resonance ($|\Delta_{off}| \gg \Omega$). On resonance, the coupling will produce an oscillation where a single photon transfers between qubit and resonator with unit probability, alternating between states with, say, the qubit in its ground state with n photons in the resonator, $|g\rangle \otimes |n\rangle = |g, n\rangle$, and the qubit in its excited state with $n-1$ photons in the resonator, $|e, n-1\rangle$; this occurs at the n-photon 'Rabi-swap' frequency $\sqrt{n}\Omega$. Off resonance, the system oscillates at a higher frequency $\sqrt{n\Omega^2+\Delta^2}$ but with reduced $|e, n-1\rangle$ probability $n\Omega^2/(n\Omega^2+\Delta^2) < 1$. This detuning dependence is shown in Fig. 1 for $n = 1$ photon and small detunings $|\Delta| \lesssim \Omega$. At our typical off-resonance operating point $\Delta_{off} \approx -25\Omega$, the photon transfer probability is only 0.0016 n, so the coupling is essentially turned off.

We determine from Fig. 1 the flux bias for on-resonance tuning ($\Delta = 0$) and the one-photon swap time. Using these parameters, we can pump photons one at a time into the resonator by repeatedly exciting the detuned qubit from $|g\rangle$ to $|e\rangle$ using a qubit microwave π-pulse, followed by a controlled-time, on-resonance photon swap[8], where we scale the swap time for the nth photon by $1/\sqrt{n}$. Precise scaling of this swap time is crucial for proper control, and was verified for up to 15 photons (see Supplementary Information).

Our goal is to synthesize arbitrary N-photon states in the resonator with the qubit in its ground state, disentangled from the resonator. Our target state for the coupled system is

$$|\psi\rangle = |g\rangle \otimes \sum_{n=0}^{N} c_n|n\rangle \quad (2)$$

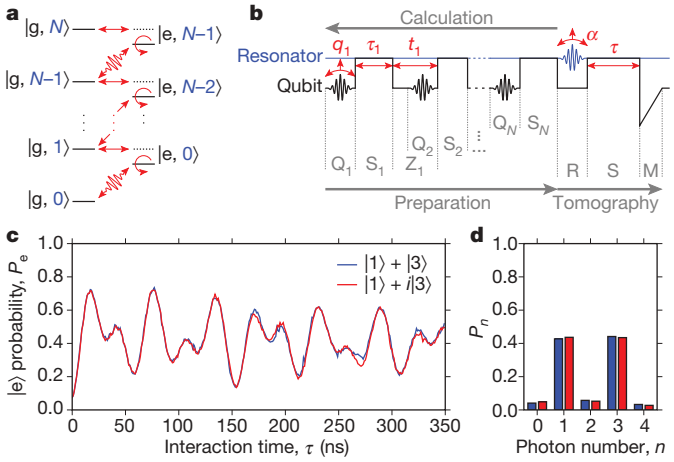

Figure 2 | Sequence to synthesize an arbitrary resonator state. **a**, Qubit–resonator energy ladder. Levels are depicted by dotted and solid lines when tuned ($\Delta = 0$) and detuned, respectively; qubit states are in black, resonator states are in blue. Three types of operations (in red) are used in state preparation: qubit drive operations Q_n, indicated by undulating lines; qubit–resonator swap operations S_n, indicated by straight horizontal lines; and phase rotations of the qubit state Z_n, indicated by circles. Each operation affects all the levels in the diagram. **b**, Microwave pulse sequence. The qubit and resonator are traced in black and blue, respectively, with qubit operations in red. The sequence is computed in reverse order by emptying energy levels from top to bottom. To descend the first step of the ladder in **a**, a swap operation S_N transfers the highest occupied resonator state to the qubit, $|g, N\rangle \rightarrow |e, N-1\rangle$. This operation also performs incomplete transfers on all the lower-lying states, as do the succeeding steps. A qubit microwave drive Q_N then transfers all the population of $|e, N-1\rangle$ to $|g, N-1\rangle$ (in general this step is not a π-pulse as $|g, N-1\rangle$ is not completely emptied by pulse S_N). For the second step down the ladder, a rotation Z_{N-1} first adjusts the phase of the qubit excited state $|e\rangle$ relative to the ground state $|g\rangle$. The succeeding swap pulse S_{N-1} can then move the entire population of $|g, N-1\rangle$ to $|e, N-2\rangle$. This sequence is repeated N times until the ground state $|g, 0\rangle$ is reached. Steps Q_n are performed with resonant qubit microwave pulses of amplitude q_n, swaps S_n achieved by bringing the qubit and resonator on resonance for time τ_n, and phase rotations Z_n completed by adjusting the detuning time t_n; see Table 1 for a detailed example. After state preparation, tomographic readout is performed: a displacement $D(-\alpha)$ of the resonator is performed by a microwave pulse R to the resonator, then the resonator state is probed by a qubit–resonator swap S for a variable interaction time τ, and finally the qubit state measured by the measurement pulse M. **c**, Plot of the qubit excited state probability P_e versus interaction time τ for the resonator states $|\psi_a\rangle = |1\rangle + |3\rangle$ (blue) and $|\psi_b\rangle = |1\rangle + i|3\rangle$ (red), taken with $\alpha = 0$. We clearly observe oscillations at the $|1\rangle$ and $|3\rangle$ Fock state frequencies. Nearly identical traces for $|\psi_a\rangle$ and $|\psi_b\rangle$ indicate the same photon number probability distribution, as expected. **d**, Photon number distributions for $|\psi_a\rangle$ (blue) and $|\psi_b\rangle$ (red). Both states are equal superpositions of $|1\rangle$ and $|3\rangle$ but the phase information that distinguishes the two states is lost.

with complex amplitude c_n for the nth Fock state. Law and Eberly[7] showed that these states can be generated by sequentially exciting the qubit into the proper superposition of $|g\rangle$ and $|e\rangle$, and then performing a partial transfer to the resonator. As illustrated in Fig. 2, and detailed in Table 1, a sequence generating the desired state can be found by solving the time-reversed problem: starting with the desired final state, we first transfer the amplitude of the highest occupied resonator Fock state to the qubit, then remove the excitation from the subsequently detuned qubit using a classical microwave signal, and repeat until the ground state $|g, 0\rangle$ is reached. The actual control signals are sequenced in the normal (un-reversed) order to generate the desired final state from the initial ground state. We note that the Law and Eberly protocol[7] assumes an adjustable phase for the qubit–resonator coupling Ω, which equation (1) does not allow; instead, we correct the relative phases of $|g, n\rangle$ and $|e, n-1\rangle$ by adjusting the time t_n over which the qubit and resonator are detuned.

To calibrate the actual microwave signals needed to implement this sequence, it is impractical to individually tune each sequence step,

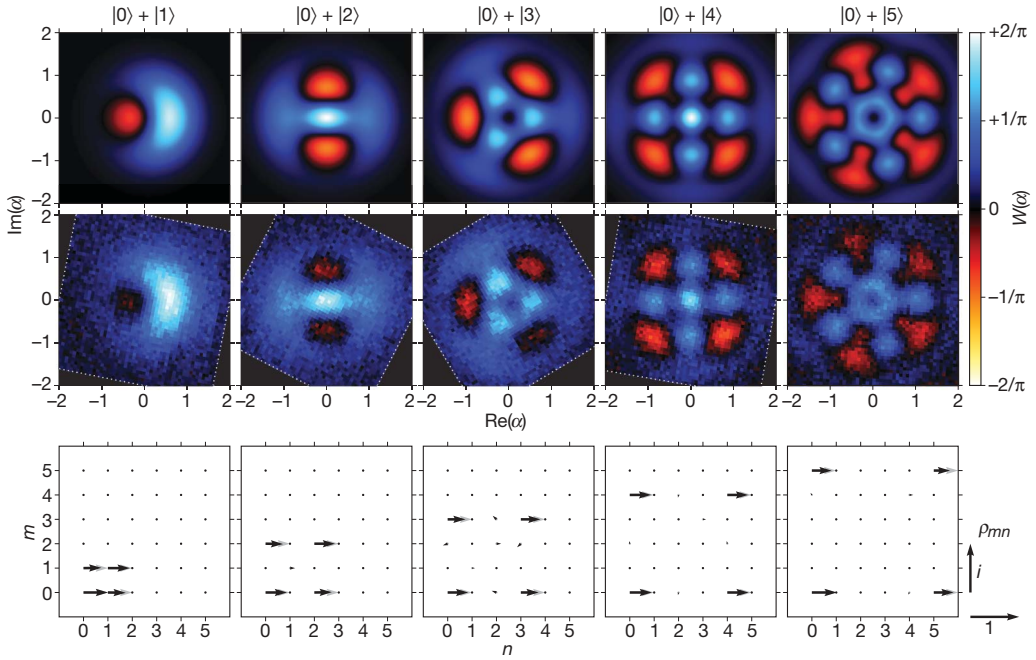

Figure 3 | Wigner tomography of superpositions of resonator Fock states $|0\rangle + |N\rangle$. The top row displays the theoretical form of the Wigner function $W(\alpha)$ as a function of the complex resonator amplitude α in photon number units, for states $N = 1$ to 5. The measured Wigner functions are shown in the middle row, with the colour scale bar on the far right. Negative quasi-probabilities are clearly measured. The experimental Wigner functions have been rotated to match theory, compensating for a phase delay between the qubit and resonator microwave lines; the measured area is bounded by a dotted white line. The bottom row displays the calculated (grey) and measured (black) values for the resonator density matrix ρ, projected onto the number states $\rho_{mn} = \langle m|\rho|n\rangle$. The magnitude and phase of ρ_{mn} is represented by the length and direction of an arrow in the complex plane (for scale, see key on right). The fidelities $F = \sqrt{\langle\psi|\rho|\psi\rangle}$ between the desired states $|\psi\rangle$ and the measured density matrices ρ are, from left to right, $F = 0.92$, 0.89, 0.88, 0.94 and 0.91. Each of the 51 by 51 pixels (61 by 61 for $N = 5$) in the Wigner function represents a local measurement. The value of $W(\alpha)$ is calculated at each pixel from 50 (41 for $N = 4$ and 5) interaction times τ, each repeated 900 times to give $P_e(\tau)$. This direct mapping of the Wigner function takes $\sim 10^8$ measurements or ~ 5 h.

because the intermediate states are quite complex and measuring them is time-consuming. Instead we perform careful calibrations of the experimental system independent of the particular state preparation (see Supplementary Information).

An initial check of the outcome of the preparation is to determine if the qubit ends up in the ground state $|g\rangle$, as desired. We find that this holds with a probability typically greater than 80%, the remaining 20% being compatible with decoherence during the preparation sequence (see Supplementary Information).

With the qubit near its ground state and not entangled with the resonator, we can use the qubit to measure the resonator state. By bringing the qubit and resonator into resonance for a variable time τ and subsequently measuring the probability P_e for the qubit excited state, we can determine[8] the n-photon probabilities $P_n = |c_n|^2$, correcting for measurement fidelity and initial qubit state probability (see Supplementary Information). In Fig. 2c we compare $P_e(\tau)$ for the experimentally prepared states $|\psi_a\rangle = |1\rangle + |3\rangle$ and $|\psi_b\rangle = |1\rangle + i|3\rangle$, showing the expected superposed oscillations corresponding to the $|1\rangle$ and $|3\rangle$ Fock states. This measurement however only yields the probabilities P_n: the relative phases of the Fock states are lost, so the states $|\psi_a\rangle$ and $|\psi_b\rangle$ cannot be distinguished.

To measure the complex amplitudes c_n, we need to probe the interference between the superposed Fock states. This may be done using Wigner tomography[19,21,24], which maps out the Wigner quasi-probability distribution $W(\alpha)$ as a function of the phase space amplitude α of the resonator (see Supplementary Information). Wigner tomography is performed by following the functional definition:

$$W(\alpha) = \frac{2}{\pi}\langle\psi|D^{\dagger}(-\alpha)\Pi\, D(-\alpha)|\psi\rangle \qquad (3)$$

The resonator state $|\psi\rangle$ is first displaced by the operator $D(-\alpha)$, implemented with a microwave drive pulse $-\alpha = (1/2)\int \Omega_r(t)\mathrm{d}t$. The photon number probabilities P_n are then measured and finally the parity $\langle\Pi\rangle = \sum_n (-1)^n P_n$ evaluated. The corresponding pulse sequence is depicted in Fig. 2b.

Calculated and measured Wigner functions are shown in Fig. 3 top and middle rows, respectively, for the resonator states $|0\rangle + |N\rangle$, with $N = 1$ to 5. The structures of the Wigner functions match well, including fine details, indicating that the superposed states are created and measured accurately. The density matrices for each state are also calculated (Fig. 3 bottom row; see Supplementary Information) and are as expected. The Wigner function of non-classical states has been measured previously, either calculated via an inverse Radon transform[18,26,27], or measured at enough points to fit the density matrix[3,28], from which the Wigner function is reconstructed. The high resolution direct mapping of the Wigner function used here is an important verification of our state preparation. The good agreement in shape shows that very pure superpositions of $|0\rangle$ and $|N\rangle$ have been created. Slight deviations in amplitude can be due to small errors in the read-out process, the relative amplitudes of the $|0\rangle$ and $|N\rangle$ states, or statistical mixtures with other Fock states.

The data in Fig. 3 do not demonstrate phase control between Fock states, as a change in the relative phase of a two-state superposition only rotates the Wigner function. The phase accuracy may be robustly demonstrated by preparing states with a superposition of three Fock states, as changing the phase of one state then changes the shape of the Wigner function. Figure 4 shows Wigner tomography for a superposition of the $|0\rangle$, $|3\rangle$ and $|6\rangle$ Fock states, where the phase of the $|3\rangle$ state has been changed in each of the five panels. The shape of the calculated and measured Wigner functions (Fig. 4 top and middle rows, respectively) again agree, including small details, indicating that precise phase control has been achieved. The calculated and measured density matrices (Fig. 4 bottom row) also match well.

In conclusion, we have generated and measured arbitrary superpositions of resonator quantum states. State preparation is deterministic and 'on-demand', requiring no projective measurements, and limited

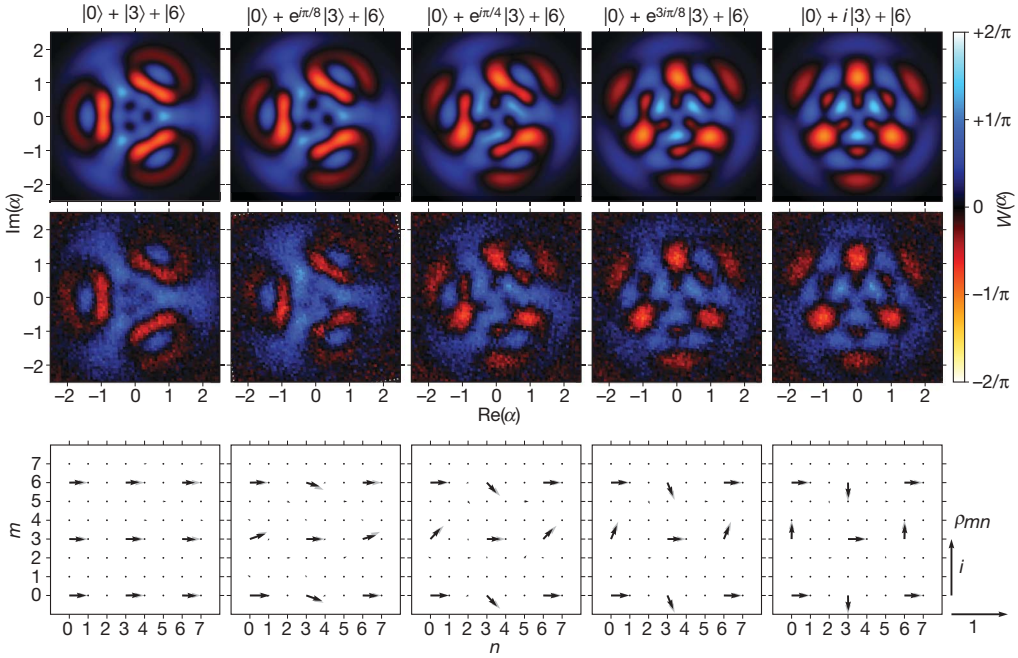

Figure 4 | Wigner tomography of the states $|0\rangle + e^{ik\pi/8}|3\rangle + |6\rangle$ for five values of phase $k = 0$ to 4. The top row is calculated, whereas the middle row shows measurements. The bottom row displays the calculated (grey) and measured (black) values for the density matrix obtained from the Wigner functions, displayed as for Fig. 3. The fidelities between the expected states and the measured density matrices are, from left to right, $F = 0.89$, 0.91, 0.91, 0.91 and 0.91.

to about ten photons, mainly by decoherence[29]. The accuracy of the prepared states demonstrates that a qubit, when controlled with high fidelity, is ideally suited for synthesizing and measuring arbitrary quantum states of light.

Received 15 January; accepted 19 March 2009.

1. Nielsen, M. A. & Chuang, I. L. *Quantum Computation and Quantum Information* (Cambridge Univ. Press, 2000).
2. Ben-Kish, A. *et al.* Experimental demonstration of a technique to generate arbitrary quantum superposition states of a harmonically bound spin-1/2 particle. *Phys. Rev. Lett.* **90,** 037902 (2003).
3. Deléglise, S. *et al.* Reconstruction of non-classical cavity field states with snapshots of their decoherence. *Nature* **455,** 510–514 (2008).
4. Houck, A. A. *et al.* Generating single microwave photons in a circuit. *Nature* **449,** 328–331 (2007).
5. Sillanpää, M. A., Park, J. I. & Simmonds, R. W. Coherent quantum state storage and transfer between two phase qubits via a resonant cavity. *Nature* **449,** 438–442 (2007).
6. Boozer, A. D., Boca, A., Miller, R., Northup, T. E. & Kimble, H. J. Reversible state transfer between light and a single trapped atom. *Phys. Rev. Lett.* **98,** 193601 (2007).
7. Law, C. K. & Eberly, J. H. Arbitrary control of a quantum electromagnetic field. *Phys. Rev. Lett.* **76,** 1055–1058 (1996).
8. Hofheinz, M. *et al.* Generation of Fock states in a superconducting quantum circuit. *Nature* **454,** 310–314 (2008).
9. Martinis, J. M., Devoret, M. H. & Clarke, J. Energy-level quantization in the zero-voltage state of a current-biased Josephson junction. *Phys. Rev. Lett.* **55,** 1543–1546 (1985).
10. Clarke, J. & Wilhelm, F. K. Superconducting quantum bits. *Nature* **453,** 1031–1042 (2008).
11. Vion, D. *et al.* Manipulating the quantum state of an electrical circuit. *Science* **296,** 886–889 (2002).
12. Niskanen, A. O. *et al.* Quantum coherent tunable coupling of superconducting qubits. *Science* **316,** 723–726 (2007).
13. Plantenberg, J. H., de Groot, P. C., Harmans, C. J. P. M. & Mooij, J. E. Demonstration of controlled-NOT quantum gates on a pair of superconducting quantum bits. *Nature* **447,** 836–839 (2007).
14. Fink, J. M. *et al.* Climbing the Jaynes-Cummings ladder and observing its $\sqrt{n}$ nonlinearity in a cavity QED system. *Nature* **454,** 315–318 (2008).
15. Steffen, M. *et al.* State tomography of capacitively shunted phase qubits with high fidelity. *Phys. Rev. Lett.* **97,** 050502 (2006).
16. Liu, Y. X. *et al.* Generation of non-classical photon states using a superconducting qubit in a quantum electrodynamic microcavity. *Europhys. Lett.* **67,** 941–947 (2004).
17. Vogel, K., Akulin, V. M. & Schleich, W. P. Quantum state engineering of the radiation field. *Phys. Rev. Lett.* **71,** 1816–1819 (1993).
18. Smithey, D. T., Beck, M., Raymer, M. G. & Faridani, A. Measurement of the Wigner distribution and the density matrix of a light mode using optical homodyne tomography: Application to squeezed states and the vacuum. *Phys. Rev. Lett.* **70,** 1244–1247 (1993).
19. Banaszek, K. & Wódkiewicz, K. Direct probing of quantum phase space by photon counting. *Phys. Rev. Lett.* **76,** 4344–4347 (1996).
20. Lutterbach, L. G. & Davidovich, L. Method for direct measurement of the Wigner function in cavity QED and ion traps. *Phys. Rev. Lett.* **78,** 2547–2550 (1997).
21. Banaszek, K., Radzewicz, C., Wódkiewicz, K. & Krasiński, J. S. Direct measurement of the Wigner function by photon counting. *Phys. Rev. A* **60,** 674–677 (1999).
22. Bertet, P. *et al.* Direct measurement of the Wigner function of a one-photon Fock state in a cavity. *Phys. Rev. Lett.* **89,** 200402 (2002).
23. Wigner, E. On the quantum correction for thermodynamic equilibrium. *Phys. Rev.* **40,** 749–759 (1932).
24. Haroche, S. & Raimond, J.-M. *Exploring the Quantum — Atoms, Cavities and Photons* (Oxford Univ. Press, 2006).
25. Neeley, M. *et al.* Transformed dissipation in superconducting quantum circuits. *Phys. Rev. B* **77,** 180508 (2008).
26. Breitenbach, G., Schiller, S. & Mlynek, J. Measurement of the quantum states of squeezed light. *Nature* **387,** 471–475 (1997).
27. Lvovsky, A. I. & Babichev, S. A. Synthesis and tomographic characterization of the displaced Fock state of light. *Phys. Rev. A* **66,** 011801 (2002).
28. Leibfried, D. *et al.* Experimental determination of the motional quantum state of a trapped atom. *Phys. Rev. Lett.* **77,** 4281–4285 (1996).
29. Wang, H. *et al.* Measurement of the decay of Fock states in a superconducting quantum circuit. *Phys. Rev. Lett.* **101,** 240401 (2008).

Supplementary Information is linked to the online version of the paper at www.nature.com/nature.

Acknowledgements Devices were made at the UCSB Nanofabrication Facility, a part of the NSF-funded National Nanotechnology Infrastructure Network. We thank M. Geller for discussions. This work was supported by IARPA (grant W911NF-04-1-0204) and by the NSF (grant CCF-0507227).

Author Contributions M.H. performed the experiments and analysed the data. H.W. improved the resonator design and fabricated the sample. J.M.M. and E.L. designed the custom electronics and M.H. developed the calibrations for it. M.A. and M.N. provided software infrastructure. All authors contributed to the fabrication process, qubit design or experimental set-up. M.H., J.M.M. and A.N.C. conceived the experiment and co-wrote the paper.

Author Information Reprints and permissions information is available at www.nature.com/reprints. Correspondence and requests for materials should be addressed to A.N.C. (Cleland@physics.ucsb.edu).